www.nature.com/cr
www.cell-research.com

Cell Research

ARTICLE

Skp2 dictates cell cycle-dependent metabolic oscillation between glycolysis and TCA cycle

Jing Liu[1,2], Yunhua Peng[2], Le Shi[2], Lixin Wan[1,3], Hiroyuki Inuzuka[1], Jiangang Long[2], Jianping Guo[1,4], Jinfang Zhang[1,5], Min Yuan[6], Shuangxi Zhang[2], Xun Wang[2,7], Jing Gao[2], Xiangpeng Dai[1], Shozo Furumoto[8], Lijun Jia[9], Pier Paolo Pandolfi[10], John M. Asara[6], William G. Kaelin Jr.[11,12], Jiankang Liu[2] and Wenyi Wei[1]

Whether glucose is predominantly metabolized via oxidative phosphorylation or glycolysis differs between quiescent versus proliferating cells, including tumor cells. However, how glucose metabolism is coordinated with cell cycle in mammalian cells remains elusive. Here, we report that mammalian cells predominantly utilize the tricarboxylic acid (TCA) cycle in G1 phase, but prefer glycolysis in S phase. Mechanistically, coupling cell cycle with metabolism is largely achieved by timely destruction of IDH1/2, key TCA cycle enzymes, in a Skp2-dependent manner. As such, depleting *SKP2* abolishes cell cycle-dependent fluctuation of IDH1 protein abundance, leading to reduced glycolysis in S phase. Furthermore, elevated Skp2 abundance in prostate cancer cells destabilizes IDH1 to favor glycolysis and subsequent tumorigenesis. Therefore, our study reveals a mechanistic link between two cancer hallmarks, aberrant cell cycle and addiction to glycolysis, and provides the underlying mechanism for the coupling of metabolic fluctuation with periodic cell cycle in mammalian cells.

Cell Research (2021) 31:80–93; https://doi.org/10.1038/s41422-020-0372-z

INTRODUCTION

Normally differentiated cells largely rely on tricarboxylic acid (TCA) cycle for converting glucose to energy, whereas proliferating cancer cells are addicted to glycolysis even when oxygen is present, a phenotype termed aerobic glycolysis or "Warburg Effect", which has been shown to benefit cancer cell growth and tumorigenesis.[1,2] Cancer cells are constantly dividing and require more metabolic intermediates, such us acetyl-CoA, to build macromolecules for their daughter cells.[3–8] Extensive investigations have revealed that many oncogenic signaling pathways, such as PKM2, HIF, AKT, Ras and Myc are critical regulatory components in the "Warburg Effect",[4–6] but the underlying mechanism(s) for the link between cell cycle and cancer cell metabolism is largely elusive. A cell cycle-coupled metabolic cycle has been reported in yeasts, where genes with metabolic functions are expressed with robust periodicity, and cells tend not to utilize oxygen for metabolism when dividing event happens,[9] so as to avoid damage to newly duplicated DNA.[10]

Ubiquitination and subsequent degradation of key cyclins dictate the normal transition of cell cycle, where APC/C (anaphase-promoting complex/cyclosome) and SCF (Skp1–Cul1–F-box protein) E3 complex ligases play a key role in this process. Several previous studies indicate a crosstalk between cell cycle regulators and glycolysis,[11–13] and several glycolytic enzymes have been reported to be regulated by cell cycle components, such as PFKFB3 (6-phosphofructo-2-kinase/fructose-2, 6-bisphosphatase-3) by SCF^{GRR1}, $SCF^{\beta\text{-}TRCP}$ and APC^{Cdh1},[12,14–16] HK2 (hexokinase 2) by cyclin D1,[17] PFKP (phosphofructokinase, platelet type) and PKM2 (pyruvate kinase M2) by cyclin D3/CDK6.[7] However, in mammalian cells, there is a lack of a systemic study about the link between cell cycle and metabolic dependence, especially TCA cycle enzymes. We previously found that $SCF^{\beta\text{-}TRCP}$ E3 ligase degrades lipin1 to promote hepatic lipogenesis in liver,[18] but little is known about whether SCF E3 ligase regulates glucose metabolism in a cell cycle-dependent manner.

In the present study, we attempted to address the mechanism of how the cell cycle machinery remodels cell metabolism, and to explore its role in tumorigenesis. Using Seahorse extracellular flux analyzer and ^{13}C-labeled metabolic flux assays, we measured the metabolic dependence in multiple cell lines after cell cycle synchronization with different methods, including nocodazole block, double thymidine block, as well as serum starvation. We found that mammalian cells predominantly utilize the TCA cycle in G1 phase, but prefer glycolysis in S phase. Importantly, coupling

[1]Department of Pathology, Beth Israel Deaconess Medical Center, Harvard Medical School, Boston, MA 02215, USA; [2]Center for Mitochondrial Biology and Medicine, The Key Laboratory of Biomedical Information Engineering of Ministry of Education, School of Life Science and Technology and Frontier Institute of Science and Technology, Xi'an Jiaotong University, Xi'an, Shaanxi 710049, China; [3]Department of Molecular Oncology, H. Lee Moffitt Cancer Center and Research Institute, Tampa, FL 33612, USA; [4]Institute of Precision Medicine, the First Affiliated Hospital, Sun Yat-sen University, Guangzhou, Guangdong 510275, China; [5]Medical Research Institute, School of Medicine, Wuhan University, Wuhan, Hubei 430071, China; [6]Cancer Research Institute, Beth Israel Deaconess Cancer Center, Department of Medicine and Pathology, Beth Israel Deaconess Medical Center, Harvard Medical School, Boston, MA 02215, USA; [7]Children's Medical Center Research Institute, University of Texas Southwestern Medical Center, Dallas, TX 75390, USA; [8]Division of Radiopharmaceutical Chemistry, Cyclotron and Radioisotope Center, Tohoku University, Sendai 980-8578, Japan; [9]Cancer Institute, Longhua Hospital, Shanghai University of Traditional Chinese Medicine, Shanghai 200032, China; [10]Division of Signal Transduction, Beth Israel Deaconess Medical Center and Department of Medicine, Harvard Medical School, Boston, MA 02215, USA; [11]Howard Hughes Medical Institute, Chevy Chase, MD, USA and [12]Department of Medical Oncology, Dana-Farber Cancer Institute, Harvard Medical School, Boston, MA, USA
Correspondence: Jiankang Liu (j.liu@mail.xjtu.edu.cn) or Wenyi Wei (wwei2@bidmc.harvard.edu)
These authors contributed equally: Jing Liu, Yunhua Peng, Le Shi

Received: 3 March 2020 Accepted: 23 June 2020
Published online: 15 July 2020

cell cycle with metabolism is largely achieved by timely destruction of IDH1/2, key TCA cycle enzymes, in a Skp2- and cyclin E/CDK2-dependent manner. Furthermore, elevated Skp2 abundance in prostate cancer cells destabilizes IDH1 to favor glycolysis and subsequent tumorigenesis. Therefore, our study reveals a mechanistic link between two cancer hallmarks, aberrant cell cycle and addiction to glycolysis.

RESULTS

Mammalian cells in distinct cell cycle phases prefer different glucose metabolism status

To understand the link between cell cycle and metabolism, we firstly synchronized HeLa cells using nocodazole and released cells into different cell cycle phases and measured the rates of glycolysis (indicated by extracellular acidification rate (ECAR)) and TCA cycle (indicated by oxygen consumption rate (OCR)) (Fig. 1a; Supplementary information, Fig. S1a). We observed that glycolysis peaked in early S phase (Fig. 1b), accompanied by a relatively lower rate of TCA cycle (Fig. 1c). In keeping with this, a relatively higher rate of glycolysis in S phase and a relatively higher rate of TCA cycle in G1 phase were also detected in synchronized HeLa cells with double thymidine block and in synchronized mouse embryonic fibroblasts (MEFs) with serum starvation (Supplementary information, Fig. S1b, c). These results suggest that glucose metabolism is likely regulated in a cell cycle-dependent manner in mammalian cells. This may be in part due to ATP needs, as cells rely mostly on the TCA cycle during G1 phase while switching to glycolysis, a less economic form of ATP production, to accumulate intermediate metabolites that are used as building blocks to synthesize biomacromolecules for subsequent DNA replication and cytokinesis.[19]

To further explore this cell cycle-dependent metabolic shift between glycolysis and TCA cycle, cells were synchronized using nocodazole and released into either G1 or S phase (Supplementary information, Fig. S1d), followed by labeling with ^{13}C6-glucose or ^{13}C5-glutamine to profile metabolic intermediates with liquid chromatography-mass spectrometry (LC-MS)[20] (Fig. 1d). Notably, cells in S phase exhibited a relatively higher glycolytic flux rate than those in G1 phase (Fig. 1e; Supplementary information, Fig. S1e), which could not be explained by differences of glucose uptake in these two cell cycle phases (Supplementary information, Fig. S1f). In contrast to the relatively fast glycolysis flux in minutes, it took ~2 h for the TCA cycle flux to reach a steady state (Supplementary information, Fig. S1g). In keeping with the metabolic switch from TCA cycle to glycolysis in S phase, we observed a reduction of TCA cycle flux for cells in S phase compared to those in G1 phase (Fig. 1f), which appeared to be independent of glutamine uptake changes (Supplementary information, Fig. S1h). Furthermore, metabolic flux through the pentose phosphate pathway (PPP) revealed by ^{13}C6-glucose labeling was also relatively higher for cells in S phase than in G1 phase, consistent with elevated synthesis of fatty acids, aromatic amino acids, and nucleic acids that is coupled with DNA duplication events in S phase (Supplementary information, Fig. S1i–k). Together, these results support a model of cell cycle-dependent metabolic switch from TCA cycle to glycolysis in S phase to facilitate DNA duplication and cell growth.

The protein levels of IDH1/2 fluctuate during cell cycle

Glycolytic and TCA cycle fluxes are both governed by a cohort of essential enzymes[21] (Supplementary information, Fig. S2a). To investigate whether the cell cycle-dependent metabolic switch from TCA cycle to glycolysis in S phase is due to the fluctuation of those enzymes, we further synchronized HeLa cells with either nocodazole or double thymidine block and monitored the protein levels of those enzymes (Supplementary information, Fig. S2b). Among those enzymes, we found that only the protein abundances of IDH1 and IDH2, but not other TCA cycle or glycolytic enzymes, fluctuated during the cell cycle in HeLa cells synchronized by either nocodazole (Fig. 2a; Supplementary information, Fig. S2c) or double thymidine block (Supplementary information, Fig. S2d), featuring relatively lower abundance of both proteins in S phase. Moreover, the fluctuation of IDH1 and IDH2 proteins could be also detected in multiple cell lines that were synchronized by different methods, including MEFs and WPMY1 cells synchronized with serum starvation and HCT116 cells synchronized with nocodazole block (Supplementary information, Fig. S2e–h). Notably, IDH1/2 mRNA levels did not fluctuate (Supplementary information, Fig. S2i, j), indicating that IDH1/2 protein stability might be regulated during the cell cycle.

Three IDH isoenzymes exist in mammalian cells: the mitochondrial NADP$^+$-dependent IDH2 and NAD$^+$-dependent IDH3 catalyze the conversion of isocitrate to α-ketoglutarate, while the cytosolic NADP$^+$-dependent IDH1 catalyzes the same reaction using cytosolic citrate.[22,23] Notably, both *Idh1*- and *Idh2*-knockout mice are viable and fertile, with noticeable mitochondrial dysfunction and increased oxidative stress, suggesting that IDH1 and IDH2 partially compensate for each other in vivo.[22,23] To understand the importance of fluctuations of IDH1 and IDH2 during the cell cycle, we measured the metabolic phenotype of *IDH1*- and *IDH2*-knockout haploid HAP1 cells generated by CRISPR/Cas9 (Fig. 2b). Compared to wild-type (WT) cells, the TCA cycle flux in *IDH2*$^{-/-}$, and to a lesser extent, *IDH1*$^{-/-}$ cells were compromised (Fig. 2c, d; Supplementary information, Fig. S2k). Consistent with this finding, loss of either *IDH1* or *IDH2* led to growth arrest in galactose-rich media ("metabolic state-dependent lethality"),[24] indicating compromised mitochondrial respiration in both *IDH1*$^{-/-}$ and *IDH2*$^{-/-}$ cells (Fig. 2e). Moreover, compared to WT cells, CRISPR/Cas9-mediated depletion of endogenous *IDH1* in HeLa cells also increased glycolysis (Fig. 2f, g), reduced TCA cycle metabolism (Fig. 2h), and increased lactate production (Supplementary information, Fig. S2l). These data suggest that cytosolic IDH1, together with mitochondrial IDH2, likely play essential roles in governing TCA cycle metabolism.

SCF^{Skp2} is the E3 ubiquitin ligase for IDH1/2 degradation

We next set out to identify the mechanism(s) responsible for S phase-specific degradation of IDH1/2. We found that endogenous IDH1 and IDH2 protein abundances, but not the mRNA levels, were markedly elevated in cells treated with either the proteasome inhibitor MG132 or the Cullin neddylation inhibitor MLN4924 (Fig. 3a; Supplementary information, Fig. S3a), implicating a Cullin-based E3 ligase in the control of IDH1/2 degradation. Among various Cullins that we examined, IDH1 and IDH2 preferentially interacted with Cullin 1, and to a lesser extent, Cullin 3 (Fig. 3b; Supplementary information, Fig. S3b). Furthermore, depleting *Cullin1*, but not *Cullin 3*, *Cullin 4A*, nor *Cullin 4B*, led to IDH1 and IDH2 accumulation (Fig. 3c; Supplementary information, Fig. S3c). Further supporting that a Cullin 1-containing E3 ligase(s) regulates IDH1 and IDH2 stability, two other essential components of the canonical SCF ubiquitin ligase complex, Skp1 and Rbx1, also interacted with IDH1 and IDH2 (Supplementary information, Fig. S3d–g). Notably, Flag-tagged IDH1 coimmunoprecipitated with GST-tagged Fbw4 and Skp2 in cells, but not other F-box proteins we examined, under ectopic overexpression conditions (Fig. 3d). However, Skp2, but not Fbw4 promoted IDH1 poly-ubiquitination in cells (Fig. 3e; Supplementary information, Fig. S3h). On the other hand, depleting *Skp2*, but not *Fbw4* dramatically elevated IDH1 in multiple cell lines, and extended half-life of IDH1 (Fig. 3f; Supplementary information, Fig. S3i–l). Moreover, endogenous Skp2 bound to IDH1 (Supplementary information, Fig. S3m). In keeping with this observation, we found that IDH1 and IDH2 were elevated in *Skp2*$^{-/-}$ MEFs compared to their WT counterparts, further implicating Skp2 as a physiological negative regulator of IDH protein stability in cells (Fig. 3g).

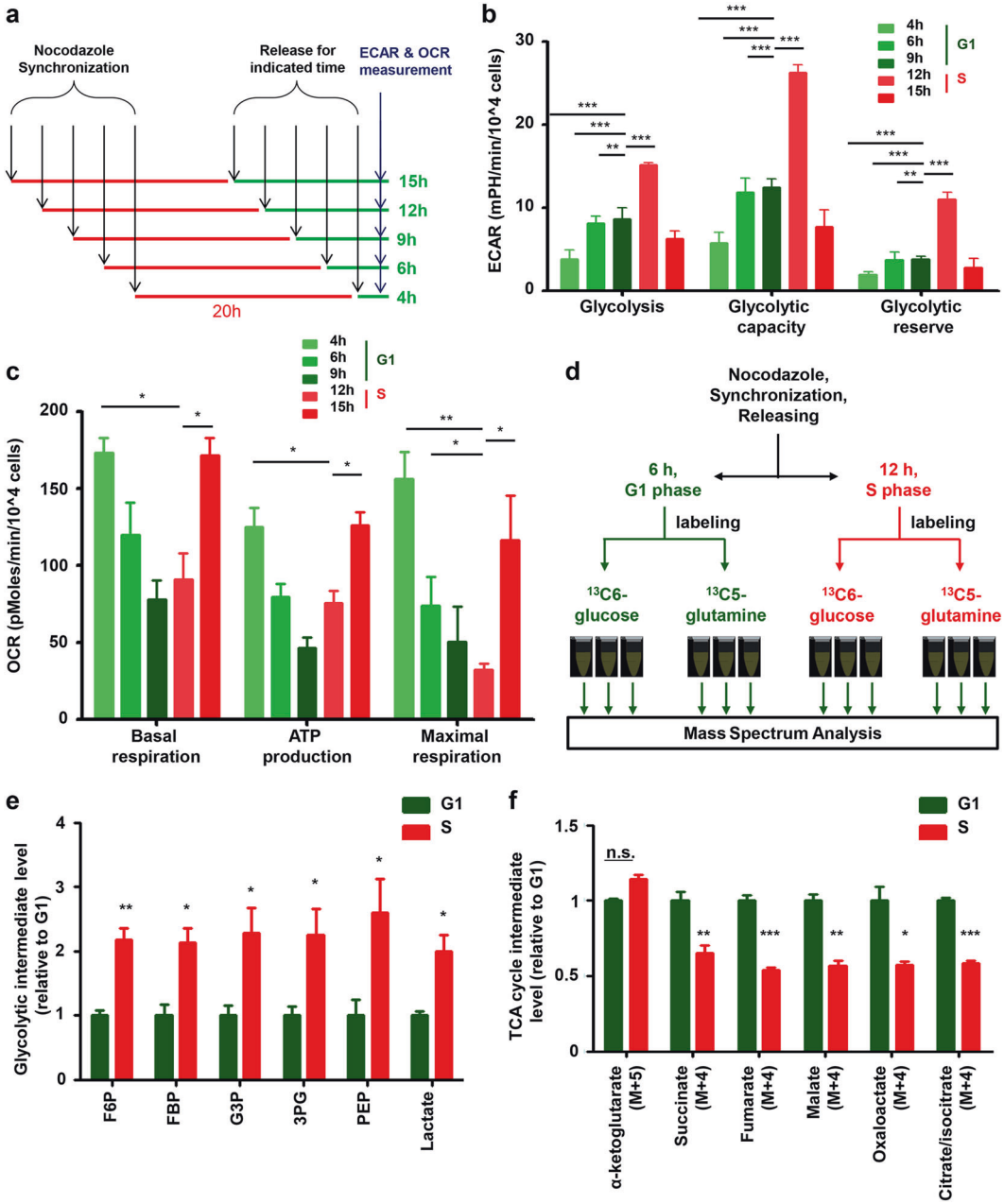

Fig. 1 Mammalian cells adopt different glucose metabolism pathways in different cell cycle stages, primarily utilizing TCA cycle in G1 phase, but relying on glycolysis in S phase. a Schematic illustration of the experimental procedure for ECAR and OCR measurements of synchronized cells. **b** Glycolysis, measured as ECAR, was found to be higher for cells in early S phase than in G1 phase. HeLa cells were synchronized by 10 μg/mL nocodazole for 20 h and subsequently released for the indicated time periods. From the ECAR curve, glycolysis (ECAR level in the presence of glucose), glycolytic capacity (stimulated glycolysis when oligomycin is used to inhibit ATP synthase), and glycolytic reserve (glycolytic capacity minus glycolysis) were calculated. $^{**}P < 0.01$, $^{***}P < 0.001$. **c** TCA cycle, measured as OCR, was found to be lower for cells in early S phase than in G1 phase. HeLa cells were synchronized by 10 μg/mL nocodazole for 20 h and subsequently released for the indicated time periods. From the OCR curve, basal respiration, ATP production (the OCR portion that is inhibited by oligomycin), and maximal respiration (stimulated OCR when antimycin A is used to inhibit electron transfer chain complex III) were calculated. $^{*}P < 0.05$, $^{**}P < 0.01$. **d** Schematic illustration of the experimental procedure for the flux assay of synchronized cells. **e** Glycolytic intermediate level was found to be higher for cells in S phase than in G1 phase. HeLa cells were synchronized with nocodazole blockage and released for 6 h (G1 phase) or 12 h (S phase), and labeled with ^{13}C-glucose for 1 min, followed by measurement of labeled glycolytic intermediates. $^{*}P < 0.05$, $^{**}P < 0.01$. **f** TCA cycle intermediate level was found to be lower for cells in S phase than in G1 phase. HeLa cells were synchronized with nocodazole and released for 6 h (G1 phase) or 12 h (S phase), and labeled with ^{13}C-glutamine for 1 h, followed by measurement of the labeled TCA cycle intermediates. n.s., not significant; $^{*}P < 0.05$, $^{**}P < 0.01$, $^{***}P < 0.001$.

To further determine whether genetic manipulation of *Skp2* affects cell cycle-dependent metabolic shift, we depleted *Skp2* in HeLa cells and measured the OCR and ECAR during the cell cycle progression of those cells. Notably, depleting *Skp2* largely abolished the cell cycle-dependent fluctuation of IDH1/2 protein abundance (Fig. 3h), which was correlated with reduced glycolytic (Fig. 3i) and OCR oscillations (Fig. 3j) in S phase. To exclude the possibility that these metabolic changes were an indirect

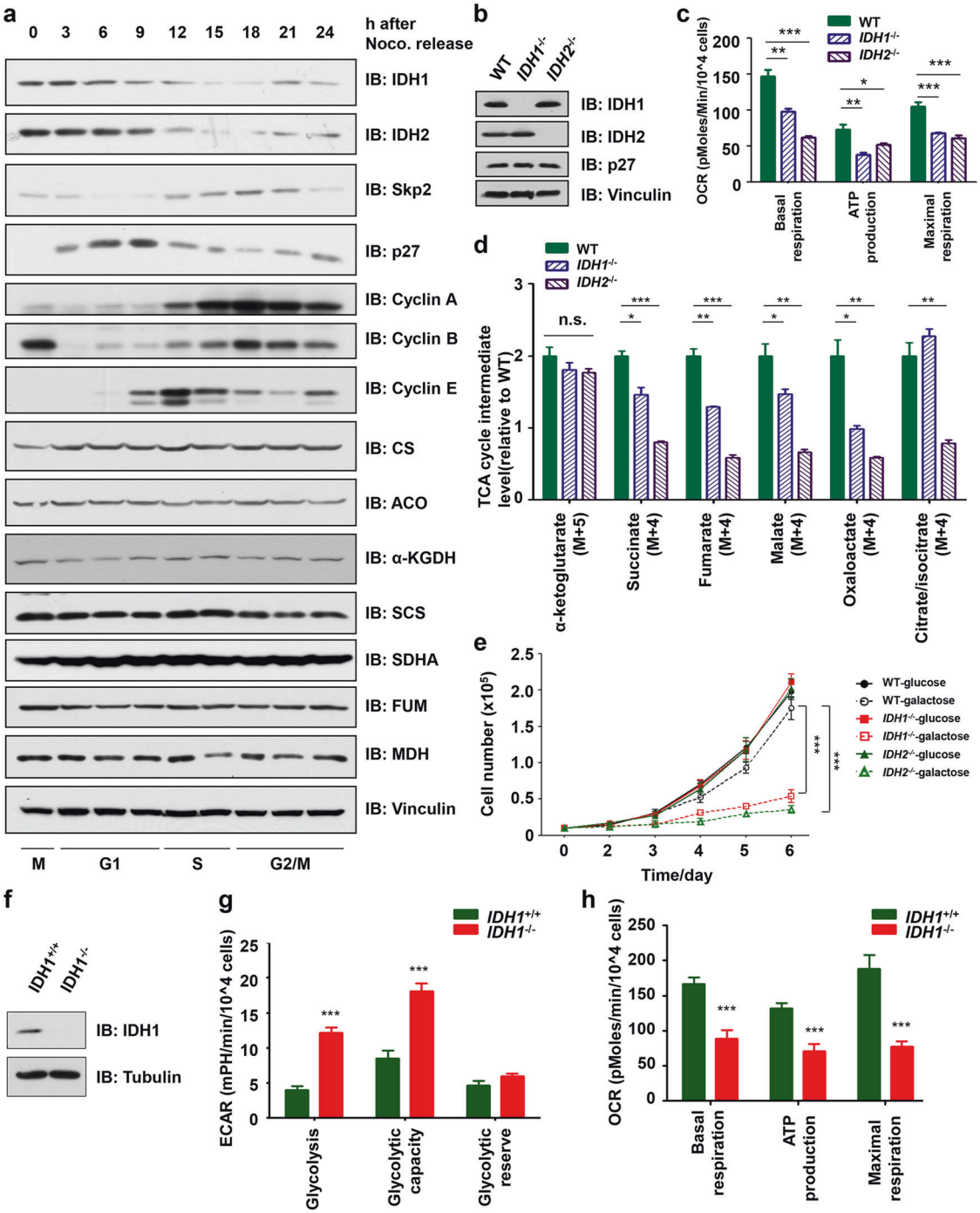

Fig. 2 The fluctuation of IDH1/2 protein abundances during cell cycle. a Protein abundance of IDH1, and to a lesser extent of IDH2, fluctuated during the cell cycle. HeLa cells were synchronized by 10 μg/mL nocodazole for 20 h and subsequently released for the indicated time periods before harvesting for immunoblot (IB) analysis. **b** IB of IDH1 and IDH2 in HAP1-*IDH1*$^{-/-}$ and HAP1-*IDH2*$^{-/-}$ cells. **c** Depletion of *IDH1* or *IDH2* compromised OCR. *$P < 0.05$, **$P < 0.01$, ***$P < 0.001$. **d** Depletion of *IDH1* or *IDH2* decreased TCA cycle intermediate level. HAP1-*IDH1*$^{-/-}$, HAP1-*IDH2*$^{-/-}$ and parental cells (WT) were labeled with ^{13}C-glutamine for 1 h followed by measurement of the labeled TCA cycle intermediates. n.s., not significant; *$P < 0.05$, **$P < 0.01$, ***$P < 0.001$. **e** Loss of either *IDH1* or *IDH2* impaired oxidative phosphorylation in HAP1 cells. HAP1-WT, HAP1-*IDH1*$^{-/-}$ and HAP1-*IDH2*$^{-/-}$ cells were cultured in DMEM with either glucose or galactose for 6 days, and the growth curve was drawn. ***$P < 0.001$. **f** IB of IDH1 in *IDH1*$^{+/+}$ and *IDH1*$^{-/-}$ HeLa cells. HeLa-*IDH1*$^{-/-}$ cells were made using CRISPR/Cas9. **g** ECAR levels of *IDH1*$^{+/+}$ and *IDH1*$^{-/-}$ HeLa cells. ***$P < 0.001$. **h** OCR levels of HeLa-*IDH1*$^{+/+}$ and *IDH1*$^{-/-}$ HeLa cells. ***$P < 0.001$.

consequence of a change in cell cycle distribution due to *Skp2* deficiency, we first synchronized cells in G1 or S phase and then performed metabolic studies (Supplementary information, Fig. S3n, o). We found that depleting *Skp2* markedly abolished cell cycle-dependent flux changes in glycolytic and TCA cycle intermediates (Fig. 3k, l). Moreover, *Skp2* depletion dramatically decreased extracellular lactate levels during S phase, providing further support for a pivotal role of Skp2 in governing the cell cycle-dependent switch to glycolytic metabolism when cells enter S phase (Supplementary information, Fig. S3p, q).

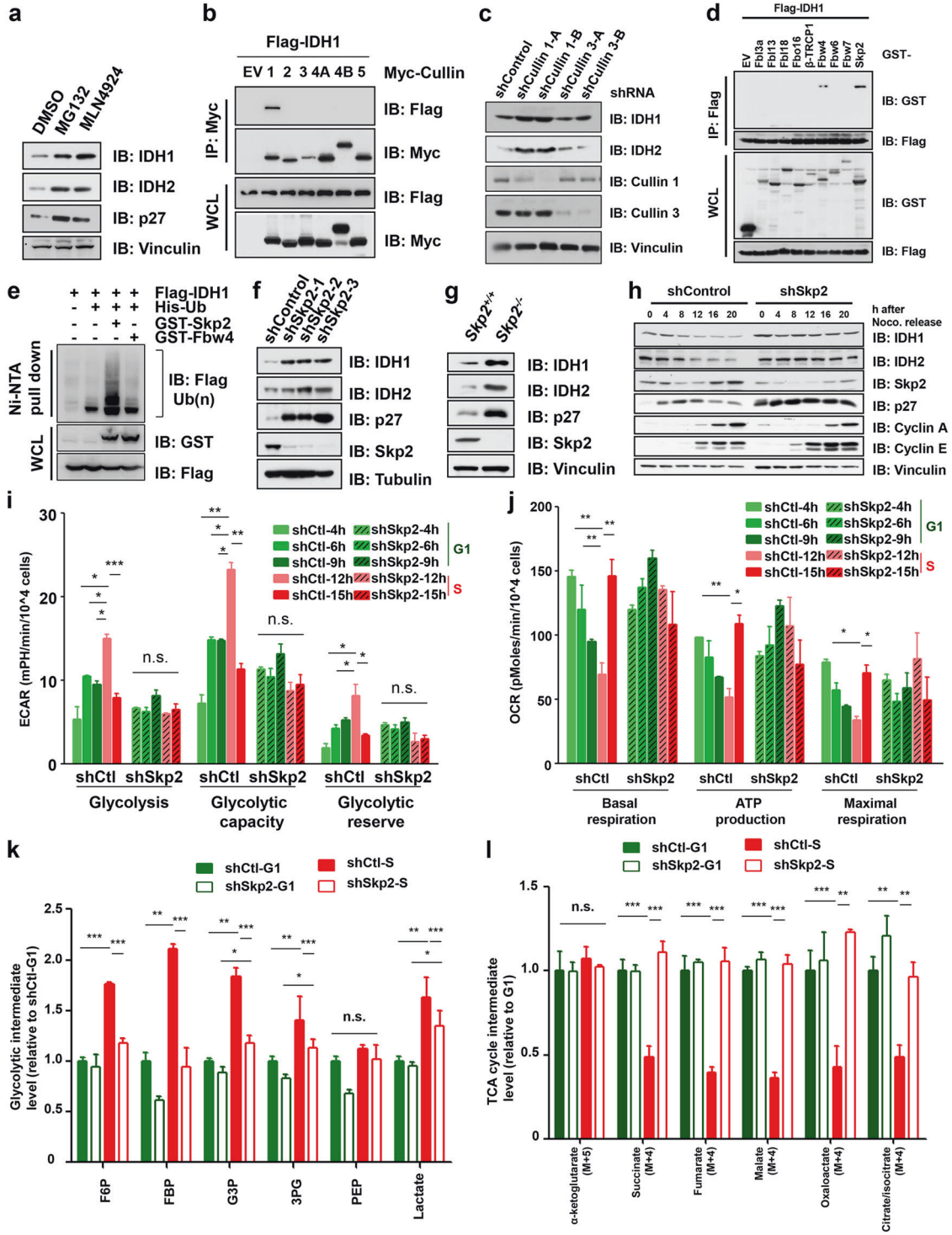

Cyclin E/CDK2 phosphorylates IDH1 at Thr157 residue

SCF^{Skp2} typically binds and ubiquitinates its downstream substrates in a phosphorylation-dependent manner.[25] We therefore examined a panel of modifying kinase(s) potentially involved in Skp2-mediated degradation of IDH1/2 in cells. Notably, cyclin E/CDK2, and to a lesser extent, cyclin A/CDK2, promoted Skp2-mediated degradation of IDH1 and IDH2 in cells (Fig. 4a; Supplementary information, Fig. S4a). In support of a physiological role for cyclin E1 and cyclin A2 as negative regulators of IDH1/2, IDH1 and IDH2 proteins were accumulated in *Ccne1*$^{-/-}$ and *Ccna2*$^{-/-}$ MEFs, but not in *Ccne2*$^{-/-}$, *Ccnd1*$^{-/-}$, *Ccnd2*$^{-/-}$ nor *Ccnd3*$^{-/-}$ MEFs, accompanied by relatively higher oxidative phosphorylation rate in *Ccne1*$^{-/-}$ MEFs (Fig. 4b; Supplementary information, Fig. S4b–d). Furthermore, CDK2 inhibition led to reduced IDH1 ubiquitination, resulting in extended half-life of the IDH1 protein (Supplementary information, Fig. S4e, f). In keeping with this observation, we found that *Ccne1*$^{-/-}$ MEFs had higher OCR level (Fig. 4c). Notably, cyclin D3/CDK6 has been recently reported to inhibit glycolysis via directly phosphorylating PFKP and PKM2,[7] whereas here we reveal a crucial role for cyclin E1/CDK2 and cyclin A2/CDK2 in suppressing TCA cycle

Fig. 3 SCF^{Skp2} promotes IDH1/2 ubiquitination and subsequent degradation, thus dictating cell cycle-dependent metabolic shift. **a** MG132 or MLN4924 treatment led to accumulation of IDH1 and IDH2. RWPE1 cells were incubated with 10 μM MG132 or 1 μM MLN4924 for 12 h, followed by IB analysis of the indicated proteins. **b** IDH1 specifically interacted with Cullin 1 in cells. IB analysis of immunoprecipitate (IP) and whole cell lysate (WCL) derived from HEK293 cells that were transfected with Flag-IDH1 and the indicated Myc-tagged Cullins for 48 h. Cells were treated with 10 μM MG132 for 12 h before harvest. **c** Knockdown of *Cullin 1*, but not *Cullin 3*, led to accumulation of IDH1 in cells. PC3 cells were infected with shControl, shCullin 1, or shCullin 3 lenti-viruses, and selected with puromycin for 3 days, followed by IB analysis of the indicated proteins. **d** IDH1 specifically interacted with two F-box proteins, Skp2, and to a lesser extent, Fbw4, in cells. IB analysis of IP and WCL derived from HEK293 cells that were transfected with Flag-IDH1 and the indicated CMV-GST-tagged F-box proteins for 48 h. Cells were treated with 10 μM MG132 for 12 h before harvest. **e** Skp2, but not Fbw4, promoted IDH1 ubiquitination in cells. IB analysis of Ni-NTA pull-down products and WCL derived from HEK293 cells transfected with the indicated constructs. Cells were treated with 30 μM MG132 for 6 h before harvest. **f** Depletion of *Skp2* in HeLa cells led to accumulation of IDH1. HeLa cells were infected with pLKO-shSkp2 or mock lenti-viruses, selected with puromycin (1 μg/mL) for 3 days to eliminate non-infected cells, and subjected to IB analysis with the indicated antibodies. **g** Genetic ablation of *Skp2* in MEFs led to a significant increase in protein abundance of IDH1 and IDH2. $Skp2^{+/+}$ and $Skp2^{-/-}$ primary MEFs were harvested and subjected to IB analysis with the indicated antibodies. **h** Depletion of endogenous *Skp2* abolished IDH1/2 abundance fluctuation during the cell cycle. HeLa cells were infected with pLKO-shSkp2 or mock lenti-viruses, and selected by puromycin for 3 days to eliminate non-infected cells. The resulting cells were synchronized by 10 μg/mL nocodazole for 20 h and subsequently released for the indicated time periods. The cells were harvested and WCL was subjected to IB analysis with the indicated antibodies. **i** Depletion of endogenous *Skp2* abolished the glycolytic peak in S phase. After releasing for the indicated time periods, cell lines generated in **h** were subjected to ECAR measurement using Seahorse XF extracellular flux analyzer. n.s., not significant; $^{*}P < 0.05$, $^{**}P < 0.01$, $^{***}P < 0.001$. **j** Depletion of endogenous *Skp2* impaired the decrease of OCR in S phase. After releasing for the indicated time periods, various cell lines generated in **h** were subjected to OCR measurement using Seahorse XF extracellular flux analyzer. $^{*}P < 0.05$, $^{**}P < 0.01$. **k** Depletion of endogenous *Skp2* eliminated the observed difference in glycolytic intermediate level between G1 phase and S phase. Various cell lines generated in **h** were synchronized and released for the indicated time periods, followed by ^{13}C-glucose labeling for 60 s. The labeled glycolytic intermediates were measured using HPLC-MS. n.s., not significant; $^{*}P < 0.05$, $^{**}P < 0.01$, $^{***}P < 0.001$. **l** Depletion of endogenous *Skp2* eliminated the observed difference in TCA cycle intermediate level between G1 phase and S phase. Various cell lines generated in **h** were synchronized and released for the indicated time periods, followed by ^{13}C-glutamine labeling for 1 h. The labeled TCA cycle intermediates were measured using HPLC-MS. n.s., not significant; $^{**}P < 0.01$, $^{***}P < 0.001$.

largely by promoting the degradation of the TCA cycle enzymes, IDH1/2. Thus, these two mechanisms might represent complementary and synergistic molecular switches for tightly controlling the metabolic cycle in a cell cycle-dependent manner.

Furthermore, we revealed that cyclin E/CDK2 phosphorylated IDH1 in vitro (Fig. 4d). To further determine the phosphorylation site in IDH1, we aligned the amino acid sequences of IDH1 and IDH2 across species (Fig. 4e); there are three potential phosphorylation sites fitting the canonical CDK2 phosphorylation consensus motif.[26] By mutating each possible CDK2 phosphorylation residue to analine (T77A, S94A, and T157A), we found that cyclin E/CDK2 primarily phosphorylated the evolutionarily conserved T157 site of IDH1 (Fig. 4f). As CDK2 exerts its kinase activity through binding either cyclin E or cyclin A,[27,28] in the latter part of this study, we primarily focused on the molecular mechanism underlying cyclin E1/CDK2-mediated degradation of IDH1/2. Importantly, the phosphorylation on T157 of exogenous IDH1 could be detected using mass spectroscopy (Supplementary information, Fig. S4g). The T157 site is also conserved in mitochondrial IDH2 (T197), suggesting that the Skp2/cyclin E/CDK2 signaling axis also negatively regulates IDH2 through this site, presumably before newly synthesized IDH2 enters the mitochondria (Supplementary information, Fig. S7b).

In keeping with a critical role of T157 in Skp2-mediated degradation of IDH1, we found that mutating T157, but not the other two SP/TP motif residues T77 or S94, to alanine abolished cyclin E/CDK2-induced Skp2 interaction with recombinant IDH1 in vitro (Fig. 4g). Moreover, synthetic peptides with amino acid sequence derived from the putative phospho-degron region in IDH1 (T157) and IDH2 (T197) bound to recombinant Skp2, but not Fbw4 in vitro, only when T157 in IDH1 or T197 in IDH2 was phosphorylated (Supplementary information, Fig. S4h–j). As a result, IDH1-T157A mutant was neither ubiquitinated by Skp2 in cells (Fig. 4h) and in vitro (Fig. 4i, j), nor degraded by Skp2 in cells (Fig. 4k; Supplementary information, Fig. S4k–m).

Non-degradable IDH1-T157A mutant abolishes metabolic shift during cell cycle and compromises cell proliferation

To explore the function of cyclin E/CDK2-dependent phosphorylation of IDH1 in metabolic oscillation during cell cycle, we constructed stable cell lines that ectopically expressed either IDH1-WT or IDH1-T157A mutant in HeLa cells. After synchronization by nocodazole block and release, unlike IDH1-WT, the protein abundance of IDH1-T157A mutant did not fluctuate in HeLa cells during the cell cycle (Fig. 5a). In keeping with the protein abundance of IDH1, the metabolic shift from TCA to glycolysis during S phase was also compromised in IDH1-T157A mutant cells (Fig. 5b, c). Compared with the cells expressing IDH1-WT, the cells expressing IDH1-T157A mutant had similar levels of glycolytic intermediates in G1 and S phases (Fig. 5d). These results indicated that the non-degradable IDH1 mutant abolished the fluctuation of IDH1 levels, leading to a lack of metabolic shift during cell cycle progression. In addition, non-degradable IDH1-T157A mutation resulted in a modest increase in G1 cells (Supplementary information, Fig. S5a).

To further understand how cell cycle-dependent metabolic shift regulates tumorigenesis, we generated several stable cell lines, including HeLa, A375, U2OS, DU145 and PC3 cells, that either express IDH-WT or IDH1-T157A mutant (Fig. 5e; Supplementary information, Fig. S5b, f, j, k). As a result of inefficiency of metabolic shift during cell cycle progression due to the abolishment of fluctuation of the IDH1-T157A mutant protein abundance, those cells expressing non-degradable IDH1-T157A mutant had compromised proliferation (Fig. 5f; Supplementary information, Fig. S5c, g). In keeping with that, those cells expressing the IDH1-T157A mutant also had compromised anchorage-independent growth indicated by crystal violet and soft agar colony formation assays (Fig. 5g–i; Supplementary information, Fig. S5d, e, h–n). Moreover, the tumors derived from PC3 cells expressing the non-degradable IDH1-T157A mutant were significantly smaller than those expressing IDH1-WT or GFP in the xenograft nude mouse model with subcutaneous injection of cancer cells (Fig. 5j, k). These data indicated that the non-degradable IDH1-T157A mutant abolished metabolic shift during cell cycle, leading to compromised tumorigenesis both in vitro and in vivo, possibly due to impaired delivery of glycolytic intermediates needed for the robust assembly of biomass during S phase to support rapid cell growth and xenograft tumorigenesis.

Reverse correlation between Skp2 and IDH1 in prostate cancer

Skp2 plays an important role in prostate tumorigenesis.[29] To further determine whether Skp2 regulates cancer cell metabolism in prostate cancer setting, we adopted a panel of prostate cancer (PrCa) cell lines, including C4-2, DU145, LNCaP, PC3, 22Rv1 and VCaP, for subsequent metabolic assays (Fig. 6a). Notably, we

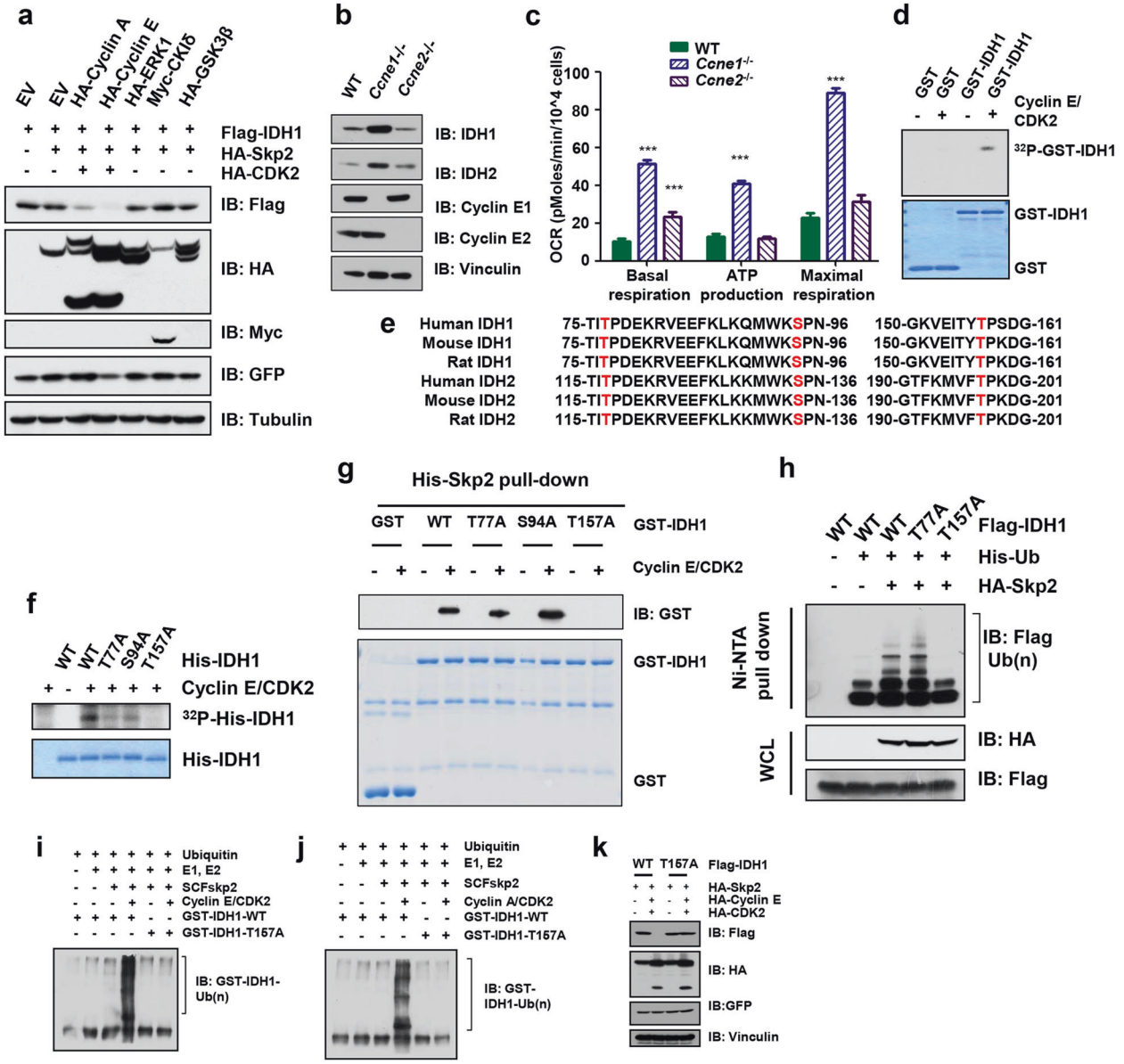

Fig. 4 Cyclin E/CDK2 phosphorylates IDH1 to trigger its ubquitination and subsequent degradation by SCF^{Skp2}. **a** Skp2 promoted IDH1 degradation in a cyclin E/CDK2- and/or cyclin A/CDK2-dependent manner in cells. IB analysis of HeLa cells after being transfected with Flag-IDH1 and the indicated constructs for 48 h. **b** Genetic ablation of *Ccne1* but not *Ccne2* in MEFs led to a significant increase in protein abundance of IDH1 and IDH2. Immortalized $Ccne1^{-/-}$, $Ccne2^{-/-}$ and WT MEFs were harvested and subjected to IB analysis with the indicated antibodies. **c** Depletion of *Ccne1* led to elevation of OCR. $Ccne1^{-/-}$, $Ccne2^{-/-}$ and WT MEFs were subjected to OCR measurement using Seahorse XF extracellular flux analyzer. ***$P < 0.001$. **d** Cyclin E/CDK2 phosphorylated IDH1 in vitro. Bacterially purified GST or GST-IDH1 recombinant proteins were incubated with purified cyclin E/CDK2 for 30 min at 30 °C using ^{32}P-γ-ATP as donor for phosphorylation, followed by SDS-PAGE. The protein input was stained with coomassie brilliant blue. **e** Alignment of the conserved TP/SP sites within IDH1 and IDH2 protein sequences among different species. **f** Identification of the T157 residue as the major site phosphorylated by cyclin E/CDK2 in vitro. Bacterially purified His-tagged IDH1 WT or mutant proteins were incubated with purified cyclin E/CDK2 for 30 min using ^{32}P-γ-ATP as donor for phosphorylation, followed by SDS-PAGE. The protein input was stained with coomassie brilliant blue. **g** Cyclin E/CDK2-dependent phosphorylation of T157 was required for IDH1 to be recognized by recombinant Skp2 in vitro. Bacterially purified recombinant GST-tagged IDH1 WT or mutant proteins were incubated with or without purified cyclin E/CDK2 for 30 min using ATP as donor for phosphorylation, followed by His-Skp2 pull-down, and then subjected to SDS-PAGE and IB analysis. The protein input was stained with coomassie brilliant blue. **h** Compared to IDH1-WT, the Skp2-dependent ubiquitination of IDH1-T157A mutant was impaired in cells. IB analysis of Ni-NTA pull-down products and WCL derived from HEK293 cells transfected with Flag-tagged IDH1 WT or mutants, together with other indicated constructs. Cells were treated with 30 μM MG132 for 6 h before harvest. **i, j** SCF^{Skp2} ubiquitinated IDH1 in vitro in a cyclin E/CDK2 (**i**) or cyclin A/CDK2 (**j**) dependent manner. IB analysis of in vitro ubiquitination assays, in which GST-IDH1-WT and GST-IDH1-T157A were purified from *E. Coli* and SCF^{Skp2} E3 ligase was purified from HEK293 cells. **k** The IDH1-T157A mutant was resistant to Skp2-dependent degradation in cells. IB analysis of WCL derived from HeLa cells transfected with Flag-IDH1-WT or Flag-IDH1-T157A and other indicated constructs.

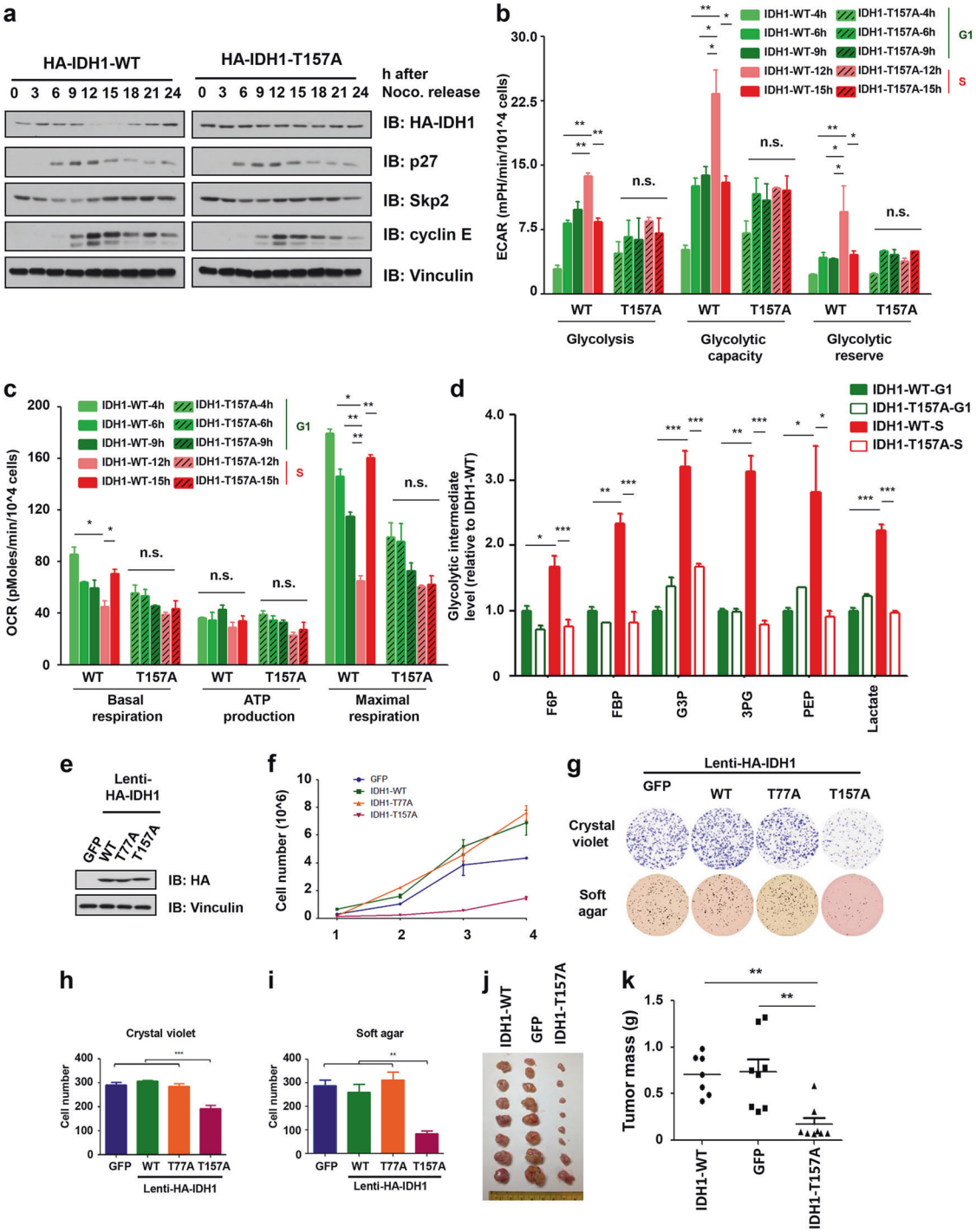

observed an inverse correlation between Skp2 and IDH1 protein abundances, but not IDH1 mRNA levels in the panel of PrCa cell lines (Fig. 6a; Supplementary information, Fig. S6a, b). Compared to four PrCa cell lines characterized by a Skp2^{low} and IDH1^{high} expression pattern (C4-2, LNCaP, VCaP, and 22Rv1), two PrCa cells characterized by a distinct Skp2^{high} and IDH1^{low} expression pattern (DU145 and PC3) displayed elevated rate of glycolysis, and reduced rate of oxidative phosphorylation (Fig. 6b, c; Supplementary information, Fig. S6c). Notably, the fluctuation of IDH1/2 protein abundance during cell cycle can also be detected in Skp2^{low} cell line 22Rv1, but not in the two Skp2^{high} cell lines, likely due to stabilization of Skp2 in Skp2^{high} cell lines that leads to less dramatic fluctuation of Skp2 itself (Supplementary information, Fig. S6d, f, g). In keeping with this notion, 22Rv1 cells also displayed cell cycle-dependent metabolic shift (Supplementary information, Fig. S6e).

To further determine the causal role of Skp2 in IDH1 protein abundance and cell metabolism, we further depleted *Skp2* in the two Skp2^{high} cells and ectopically expressed Skp2 in three Skp2^{low} cells (Fig. 6d, g). Importantly, depletion of endogenous *Skp2* in the two Skp2^{high} cells increased p27 and IDH1/2 protein levels (Fig. 6d), resulting in reduced glycolysis (Fig. 6e) and increased oxidative phosphorylation (Fig. 6f). By contrast, ectopic expression of Skp2 in Skp2^{low} cells, such as LNCaP, C4-2 and 22Rv1, reduced

Fig. 5 Non-degradable IDH1 is resistant to cell cycle-dependent fluctuation in abundance, and restricts cell proliferation. a Compared to IDH1-WT, the IDH1-T157A mutant escaped from cell cycle-dependent degradation, thereby becoming stabilized across different cell cycle phases. HeLa cells were infected with HA-IDH1-WT or HA-IDH1-T157A lenti-viruses and selected with hygromycin B (200 μg/mL) for 3 days. The stable cell lines were synchronized by nocodazole blockage for 20 h and released for the indicated time periods, followed by IB analysis with the indicate antibodies. **b** Compared to IDH1-WT, ectopic expression of the IDH1-T157A mutant significantly reduced the glycolytic peak in S phase. Various cell lines generated in **a** were synchronized by nocodazole blockage for 20 h and released for the indicated time periods, followed by ECAR measurements with Seahorse XF extracellular flux analyzer. n.s., not significant; $^{*}P < 0.05$, $^{**}P < 0.01$. **c** Compared to IDH1-WT, ectopic expression of the IDH1-T157A mutant was incapable of reducing TCA cycle in S phase. Various cell lines generated in **a** were synchronized by nocodazole blockage for 20 h and released for the indicated time periods, followed by OCR measurements with Seahorse XF extracellular flux analyzer. n.s., not significant; $^{*}P < 0.05$, $^{**}P < 0.01$. **d** Compared to IDH1-WT, ectopic expression of the IDH1-T157A mutant significantly reduced the glycolytic intermediates level in S phase. Various cell lines generated in **a** were synchronized and released for the indicated time periods, followed by ^{13}C-glucose labeling for 60 s. The labeled glycolytic intermediates were measured using HPLC-MS. $^{*}P < 0.05$, $^{**}P < 0.01$, $^{***}P < 0.001$. **e** IB analysis of the indicated proteins in HeLa stable cell lines. **f** Compared to IDH1-WT, ectopic expression of the IDH1-T157A mutant suppressed cell growth. **g** Compared to IDH1-WT, ectopic expression of the IDH1-T157A mutant compromised transformation ability. Representative images showing colony growth or anchorage-independent growth. **h, i** Quantification of the colony numbers in colony growth (**h**) or soft agar assay (**i**). $^{**}P < 0.01$, $^{***}P < 0.001$. **j** Image of xenograft tumor derived from 22Rv1 cells that expressed either GFP, IDH1-WT or IDH1-T157A mutant. **k** Quantification of xenograft tumor mass derived from 22Rv1 cells that expressed either GFP, IDH1-WT or IDH1-T157A mutant as in **j**. $^{**}P < 0.01$.

p27 and IDH1/2 protein levels (Fig. 6g), leading to increased glycolysis (Fig. 6h) and reduced oxidative phosphorylation (Fig. 6i). These results provide further support for a critical role of Skp2 in destabilizing IDH1/2, thereby coupling metabolism to cell cycle progression.

Skp2 inhibition leads to IDH1/2 accumulation and renders metabolic shift from glycolysis to TCA cycle

To further determine whether targeting the Skp2–IDH1 axis provides therapeutic possibility for prostate cancer, we treated 22Rv1 and LNCaP cells with the Skp2 inhibitor, SKPin C1.[30] Notably, SKPin C1 significantly stabilized both IDH1 and IDH2 in 22Rv1 and LNCaP cells in a dose-dependent manner (Fig. 7a; Supplementary information, Fig. S7a). As expected, IDH1 was cytosolic regardless of SKPin C1 treatment (Supplementary information, Fig. S7b). However, IDH2, which is normally mitochondrial, was detected in the cytoplasm after SKPin C1 treatment, suggesting that SCF^{Skp2}-mediated degradation of IDH2 possibly occurs before its translocation into the mitochondria (Supplementary information, Fig. S7c). Moreover, SKPin C1 treatment phenocopied the effects of expressing the non-degradable T157A-IDH1 mutant with respect to cellular proliferation (Fig. 7b). These effects were on target because they were largely abolished in cells lacking *Skp2* (Fig. 7c). Furthermore, SKPin C1 treatment led to a shift from glycolysis to TCA cycle, similar to genetic depletion of *Skp2* (Fig. 7d, e); this effect was IDH1/2 dependent because it was largely abolished in cells lacking *IDH1* or *IDH2* (Fig. 7d–f).

p27, which arrests cell cycle in G1 phase by inhibiting CDK kinase activities, is one of the best-characterized Skp2 ubiquitin substrates.[31] Importantly, depleting *P27* in multiple cell lines did not phenocopy the effects of increasing Skp2 with respect to IDH1/2 abundance (Supplementary information, Fig. S7c, d) or cell metabolism (Supplementary information, Fig. S7e, f), thus arguing against the possibility that the effects of Skp2 on IDH1/2 stability and the shift to glycolysis in S phase were indirectly mediated by fluctuations in p27 levels (Supplementary information, Fig. S7g). Moreover, depleting *IDH1* in *Skp2*-depleted cells partially rescued their metabolic phenotype (redirecting cell metabolism in favor of glycolysis), even in the G1 phase (Fig. 7g, h; Supplementary information, Fig. S7h), but did not rescue their colony growth ability (Supplementary information, Fig. S7i, j). It is therefore likely that degradation of both IDH and p27 contributes to the oncogenic role of Skp2 (Fig. 7i).

DISCUSSION

Cancer cells are quickly divided and are in high demand of biomacromolecules, including lipids, nucleotides and amino acids to prepare for the DNA replication in S phase and subsequent cell division.[3–8] In yeast, the cell metabolism is coordinated with cell division; the gene expression of metabolic enzymes fluctuate with robust periodicity, particularly, the expression of genes related to oxygen consumption is repressed during division period.[9] To date, several lines of evidence advocate a bi-directional interplay between the cell cycle and metabolic machineries. On one hand, key glycolytic enzymes, including HK2, PFKFB3, PFKP, and PKM2, are directly regulated in a cell cycle-dependent manner.[7,12,14–17] Mechanistically, the *HK2* gene expression is regulated in a cyclin D1-dependent manner,[17] while the enzyme activities of PFKP and PKM2 are regulated by cyclin D3/CDK6-dependent phosphorylation events during the cell cycle.[7] Moreover, the glycolysis-promoting enzyme PFKFB3 is ubiquitinated by several E3 ligases, including SCF^{GRR1}, $SCF^{\beta\text{-}TRCP}$ and APC^{Cdh1}, during the cell cycle.[11,12,14–16] Besides, the regulation of cellular metabolism dependence is also critical for maintaining stemness of stem cells. For example, Fbxo15, another F-box protein, has been reported to control the mitochondrial biogenesis and metabolism in embryonic stem cells via degrading KBP (KIF1-binding protein).[32] On the other hand, a perturbed metabolic state can also compromise cell cycle progression.[33]

To systematically analyze the metabolic fluctuation during cell cycle, we synchronized several cells with various methods and traced cell metabolism by using Seahorse extracellular analyzer and ^{13}C-glucose/glutamine labeling flux assays. The metabolic results indicate that in S phase, cells shift to high rates of glycolysis and low rates of TCA cycle to enable more flux of intermediates into the biomass synthesis pathways (Fig. 1; Supplementary information, Fig. S1). By monitoring the protein expressions of all enzymes in glycolysis and TCA cycle for the synchronized cells in different cell cycle phases, we found that only the abundance of the rate-limiting enzymes in TCA cycle, namely IDH1/2, fluctuated during cell cycle (Fig. 2; Supplementary information, Fig. S2). We further found that the protein stability of IDH1/2 was regulated by SCF^{Skp2} E3 ubiquitin ligase (Fig. 3; Supplementary information, Fig. S3). Specifically, during the G1/S transition, accumulated cyclin E activates CDK2,[27] which in turn phosphorylates IDH1 at the conserved Thr157 residue, leading to its recognition and subsequent ubiquitination by SCF^{Skp2} E3 ligase (Figs. 4, 5; Supplementary information, Figs. S4, S5).

Given that Skp2 plays a pivotal oncogenic role in prostate cancer,[29] we further explored the pathological effect of Skp2–IDH1 axis in PrCa setting. Notably, we found that the protein abundance of IDH1 was inversely correlated with that of Skp2, and the Skp2–IDH1 signaling axis contributed to the dictating of the distinctive cancer "Warburg" metabolic phenotype (Fig. 6; Supplementary information, Fig. S6). This study therefore reveals a novel oncogenic role of Skp2 independent of its other biological substrates such as p27 in cell cycle regulation,

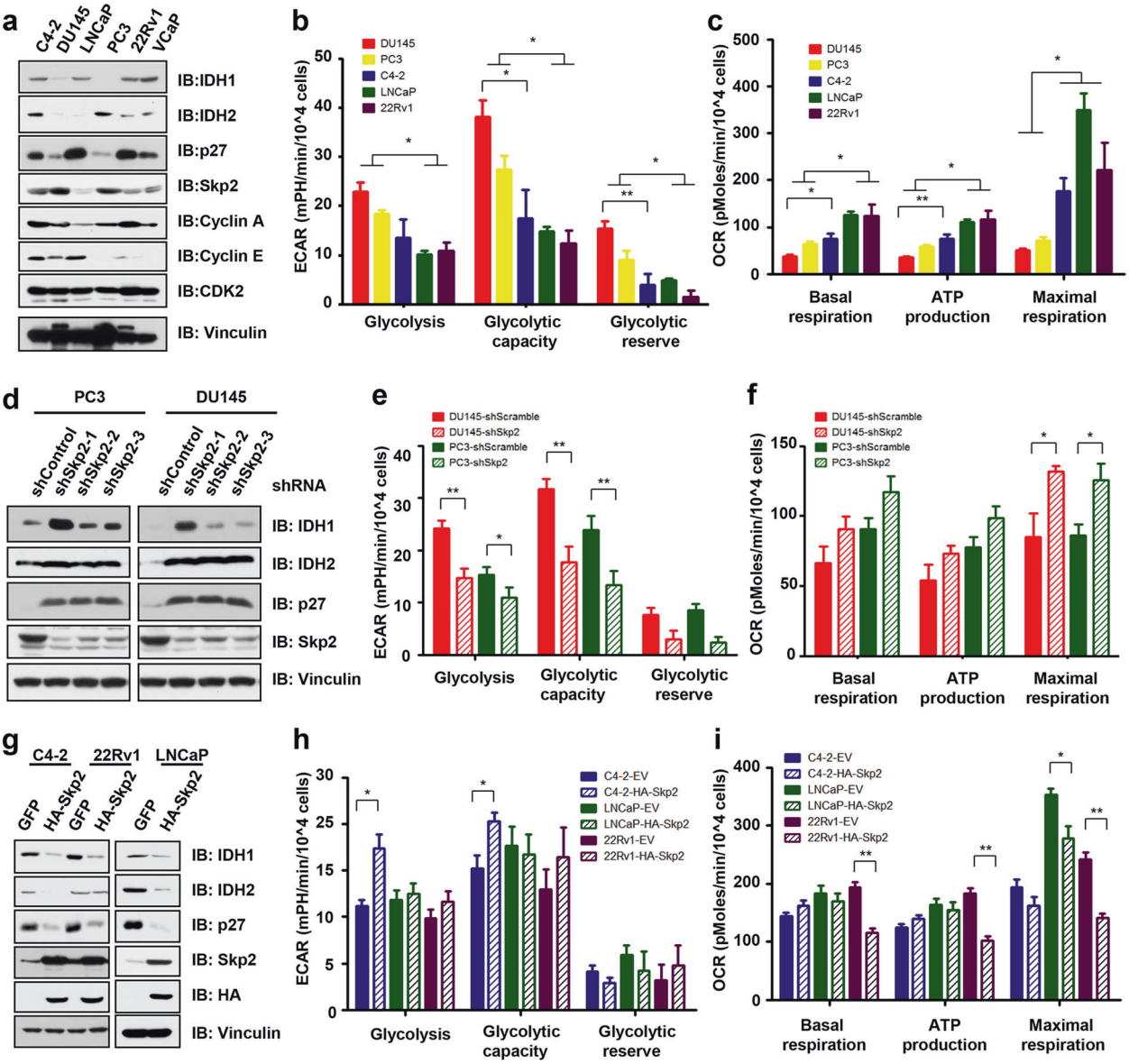

Fig. 6 Skp2 dedicates the metabolic phenotypes of prostate cancer cell lines in part by promoting IDH1 degradation. a There was an inverse correlation between the protein abundance of Skp2 and IDH1 in a panel of prostate cancer (PrCa) cell lines. IB analysis of C4-2, DU145, LNCaP, PC3, 22Rv1 and VCaP with the indicated antibodies. **b** ECAR analysis of different PrCa cell lines as listed in **a**. $^{*}P < 0.05$, $^{**}P < 0.01$. **c** OCR analysis of different PrCa cell lines as listed in **a**. $^{*}P < 0.05$, $^{**}P < 0.01$. **d** Depletion of endogenous *Skp2* in Skp2^{high} cells led to a significant elevation of IDH1 protein abundance. Two Skp2^{high} cells, PC3 and DU145 were infected with pLKO-shSkp2 or shControl lentiviruses, selected for 3 days, and harvested for IB analysis. **e** ECAR analysis of PC3 and DU145 with or without depletion of endogenous *SKP2*. $^{*}P < 0.05$, $^{**}P < 0.01$. **f** OCR analysis of PC3 and DU145 with or without depletion of endogenous *SKP2*. $^{*}P < 0.05$. **g** Enforced ectopic expression of Skp2 in Skp2^{low} cells led to elevated IDH1 degradation. Skp2^{low} cells, LNCaP, C4-2 and 22Rv1 were infected with HA-Skp2 or GFP lentiviruses, selected by puromycin for 3 days, and harvested for IB analysis. **h** ECAR analysis of LNCaP, C4-2 and 22Rv1 with or without ectopic expression of Skp2. $^{*}P < 0.05$. **i** OCR analysis of LNCaP, C4-2 and 22Rv1 with or without ectopic expression of Skp2. $^{*}P < 0.05$, $^{**}P < 0.01$.

by promoting the metabolic switch from utilization of TCA cycle to glycolysis, landing further support for the notion that targeting Skp2 may provide a potent anti-cancer therapy in part by suppressing cancer metabolism (Fig. 7; Supplementary information, Fig. S7).

MATERIALS AND METHODS

Cell culture

Human embryonic kidney 293 (HEK293) cells, HEK293FT, HeLa, DLD1, HCT116, U2OS, A375, VCaP, HAP1 cells and MEFs were maintained in Dulbecco's Modified Eagle's Medium (DMEM) containing 10% fetal bovine serum (FBS), 100 units of penicillin and 100 mg/mL streptomycin. PC3, DU145, 22Rv1, LNCaP and C4-2 cells were cultured in RPMI1640 containing 10% FBS, 100 units of penicillin and 100 mg/mL streptomycin. RWPE cells were maintained in keratinocyte serum free medium (K-SFM, Invitrogen, 44019). *Skp2*$^{+/+}$ and *Skp2*$^{-/-}$ MEFs were described previously.[34] *Ccna2*$^{f/f}$, *Ccne1*$^{-/-}$*Ccne2*$^{-/-}$, *Ccne1*$^{-/-}$, *Ccne2*$^{-/-}$, *Ccnd1*$^{-/-}$, *Ccnd2*$^{-/-}$ and *Ccnd3*$^{-/-}$ MEFs were gifts from Dr. Piotr Sicinski. HAP1-*IDH1*$^{-/-}$ (HZGHC003323c006) and HAP1-*IDH2*$^{-/-}$ (HZGHC000919c010) cells were purchased from Horizon Discovery. HAP1 is a near-haploid human cell line that was derived from KBM-7, a chronic myelogenous leukemia (CML) cell line.[35] HeLa-*IDH1*$^{-/-}$ cells were generated using CRISPR/Cas9 with a guide sequence of 5′-TACGAAATATTCTGGGTGGC-3′.[36] Cell culture transfection, lentiviral

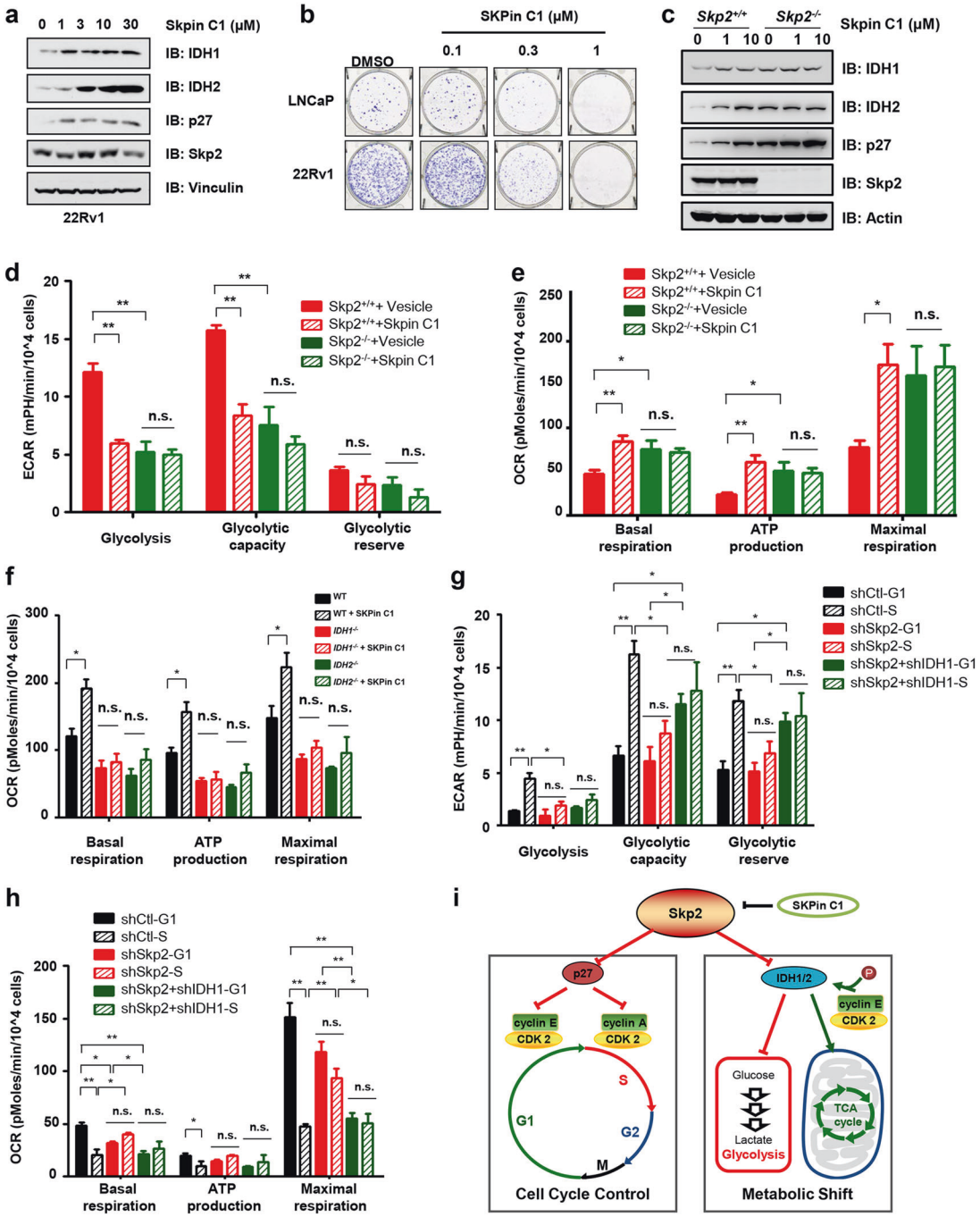

Fig. 7 Skp2 inhibitor represses prostate cancer via shifting cell metabolism from glycolysis to TCA cycle. a The treatment of Skp2 inhibitor SKPin C1 led to a robust accumulation of IDH1 and IDH2 in cells. 22Rv1 cells were treated with 0, 1, 3, 10, or 30 μM SKPin C1 for 24 h, and then harvested for IB analysis. **b** SKPin C1 blocked the colony growth of PrCa cells, LNCaP and 22Rv1. LNCaP and 22Rv1 cells were planted in 6-well plate (1500 cell/well), treated with 0.1, 0.3, or 1 μM Skin C1 for 7 days, and transferred to fresh media for another 3 weeks. **c** Depletion of *Skp2* abolished the effect of SKPin C1 on IDH1 and IDH2 abundances. HAP1-*Skp2*$^{+/+}$ and HAP1-*Skp2*$^{-/-}$ cells were treated with the indicated concentrations of SKPin C1 for 24 h, followed by IB analysis of the indicated proteins. **d** Depletion of *Skp2* abolished the effect of SKPin C1 on ECAR. n.s., not significant; $^{**}P < 0.01$. **e** Depletion of *Skp2* abolished the effect of SKPin C1 on OCR. n.s., not significant; $^{*}P < 0.05$, $^{**}P < 0.01$. **f** Depletion of endogenous *IDH1* or *IDH2* abolished the effects of SKPin C1 on OCR. HAP1-*IDH1*$^{-/-}$, HAP1-*IDH2*$^{-/-}$ and parental cells were treated with 3 μM SKPin C1 for 24 h, followed by OCR analysis with Seahorse XF 24 analyzer. n.s., not significant; $^{*}P < 0.05$. **g**, **h** Depletion of endogenous *Skp2* rendered a metabolic profile of G1 phase, while further depletion of *IDH1* resulted in a metabolic profile more similar to S phase as indicated by ECAR (**g**) and OCR (**h**). n.s., not significant; $^{*}P < 0.05$, $^{**}P < 0.01$. **i** Schematic illustration of the working model for SKPin C1 in regulating cell cycle and metabolic shift via targeting p27 and IDH1/2, respectively.

packaging and subsequent infection of various cell lines were performed according to the protocol described previously.[37] To determine the proliferation ability of HAP1 after depletion of IDH1 or IDH2, cells were cultured in H-DMEM, then transferred into DMEM without glucose (Thermo Fisher, 11966025) after adding either 25 mM of D-glucose or D-galactose.

HeLa, HCT116, WPMY1, 22Rv1, DU145, PC3 cells and MEFs were used for synchronization. HeLa cells, which have low endogenous

Skp2 activity, were used for ectopic expression-based degradation assays. HEK293 cell line was used for ubiquitination assays and co-IP assays to define the interaction between two ectopically expressed proteins, which is the most frequently used cell line for this type of experiment. Human prostate cancer cells, DU145, PC3, LNCaP, VCaP, 22Rv1 and C4-2, were used for evaluating endogenous Skp2 and IDH1 levels, as well as Skp2 knockdown and Skp2 overexpression. HAP1, LNCaP, and 22Rv1 cells were also used for treatments with Skp2 inhibitor, SKPin C1.

Plasmid construction
Skp2 cDNA was subcloned into CMV-GST, pcDNA3-HA and Lenti-puro-HA vectors via *Bam*HI and *Xho*I sites. IDH1-WT cDNA was subcloned into pET28a-His, pGEX-GST, Flag-CMV and Lenti-hygro-HA vectors via *Bam*HI and *Xho*I sites. Site-directed mutagenesis to generate various IDH1 degron mutants was performed using the QuikChange XL Site-Directed Mutagenesis Kit (Stratagene) according to the manufacturer's instructions. HA-cyclin A, HA-cyclin E, HA-CDK2, HA-ERK1, HA-GSK3β and HA-Rbx1 were generated by cloning the corresponding cDNAs into pcDNA3-HA vector via *Bam*HI and *Xho*I sites. CMV-GST-Fbl3a, CMV-GST-Fbl13, CMV-GST-Fbl18, CMV-GST-Fbo16, CMV-GST-β-TRCP1, CMV-GST-Fbw4, CMV-GST-Fbw6, CMV-GST-Fbw7 and CMV-GST-Skp2 were gifted from Dr. Wade Harper. Myc-cullin 1, Myc-cullin 2, Myc-cullin 3, Myc-cullin 4A, Myc-cullin 4B and Myc-cullin 5 were gifted from Dr. James DeCaprio. The lentiviral vectors containing Skp2 and p27 shRNAs were described before.[34] The lentiviral vectors containing cullin 1, cullin 3 and Fbw4 shRNAs were purchased from Open biosystem.

Cell cycle synchronization
Cell synchronization with nocodazole arrest, double thymidine block or serum starvation was described previously.[38,39] Briefly, HeLa cells or HCT116 cells were incubated with 10 μg/mL of nocodazole for 20 h, followed by knocking of dish on hard surface to dislodge mitotic cells and washing with PBS for 3 times. The cells were released for the indicated time periods before harvest. For double thymidine blocking, HeLa, 22Rv1, PC3 or DU145 cells were incubated with 2 mM thymidine for 16 h, then the thymidine was washed away with PBS and cells were grown in fresh media for 9 h, followed by the second round of 2 mM thymidine treatment for 15 h. After that, the cells were washed with PBS for 3 times and released for the indicated time periods before harvest. For serum starvation, MEFs and WPMY1 cells were cultured in serum-free media for 48 h, and then transferred into H-DMEM with 10% FBS for the indicated time periods before harvest.

Seahorse XF24 extracellular bioenergetics analysis
OCR and ECAR were measured using Seahorse XF24 analyzer (Boston, MA, USA). The cell numbers and FCCP concentration were optimized based on previous reports and titration experiments. OCR assays used Seahorse XF basal media containing 25 mM glucose, 1 mM sodium pyruvate and 2 mM glutamine, while ECAR assays used Seahorse XF basal media containing no glucose, no pyruvate and 2 mM glutamine. For OCR assays, the final concentrations of oligomycin, FCCP and antimycin A were 1, 0.3 and 1 μM, respectively, unless indicated otherwise. For ECAR assays, the final concentrations of glucose, oligomycin and 2-DG were 10 mM, 1 μM and 50 mM, respectively, unless indicated otherwise. After the measurement, cells were trypsined and counted, and all data were normalized with cell number.

Immunoblot (IB) and immunoprecipitation (IP) analyses
Cells were lysed in EBC buffer (50 mM Tris, pH 7.5, 120 mM NaCl, 0.5% NP-40) supplemented with protease inhibitors (cOmplete Mini, Roche) and phosphatase inhibitors (phosphatase inhibitor cocktail set I and II, Calbiochem). The protein concentrations of the lysates were measured using the Bio-Rad protein assay on a Beckman Coulter DU-800 spectrophotometer. The lysates were then resolved by SDS-PAGE and immunoblotted with the indicated antibodies. For immunoprecipitation, 1 mg lysates were incubated with the appropriate sepharose beads for 4 h at 4 °C. Immuno-complexes were washed four times with NETN buffer (20 mM Tris, pH 8.0, 100 mM NaCl, 1 mM EDTA and 0.5% NP-40) before being resolved by SDS-PAGE and immunoblotted with the indicated antibodies.

In vitro kinase assay
IDH1 in vitro kinase assays were performed as previously reported.[40] Briefly, His-IDH1 was expressed in BL21 *E. coli* and purified using Ni-NTA (Ni-nitrilotriacetic acid) agarose according to the manufacturer's instructions. One microgram of His-tagged IDH1 WT or mutant protein was incubated in the absence or presence of cyclin E/Cdk2 kinase in kinase assay buffer (10 mM HEPES, pH 8.0, 10 mM $MgCl_2$, 1 mM dithiothreitol, 0.1 mM ATP). The reaction was initiated by the addition of 10× kinase assay buffer in a volume of 30 μL for 45 min at 30 °C followed by the addition of SDS-PAGE sample buffer to stop the reaction. The reaction products were resolved by SDS-PAGE.

In vitro pull-down assay
His-Skp2 and GST-IDH1 were expressed in BL21 *E. coli* and purified using Ni-NTA agarose or Glutathione Sepharose 4B according to the manufacturer's instructions. The GST-IDH1 proteins (2 μg) were eluted using elution buffer (50 mM Tris-HCl, pH 8.0, 10 mM reduced glutathione) and incubated with or without cyclin E/Cdk2 in kinase assay buffer for 1 h. Then, the reaction solution was added with His-Skp2 beads (1 μg) and incubated for 3 h at 4 °C followed by the addition of SDS-PAGE sample buffer to stop the reaction. The reaction products were resolved by SDS-PAGE.

In vivo ubiquitination assay
Denatured in vivo ubiquitination assays were performed as previously described.[39] Briefly, HEK293 cells were transfected with Flag-IDH1, His-ubiquitin and HA-Skp2. 48 h after transfection, 30 μM MG132 was added to block proteasome degradation for 6 h and cells were harvested in denatured buffer (6 M guanidine-HCl, pH 8.0, 0.1 M Na_2HPO_4/NaH_2PO_4, 10 mM imidazole). After sonication, the ubiquitinated proteins were purified by incubation with Ni-NTA matrices for 3 h at room temperature. The pull-down products were sequentially washed twice in buffer A, twice in buffer A/TI mixture (buffer A: buffer TI = 1:3) and once in buffer TI (25 mM Tris-HCl, pH 6.8, 20 mM imidazole). The poly-ubiquitinated proteins were separated by SDS-PAGE for IB analyses.

In vitro ubiquitination assay
The in vitro ubiquitination assays were performed as previously described.[40] To purify the SCF^{Skp2} E3 ligase complex, 293 T cells were transfected with vectors encoding Flag-Skp2, HA-Cul1, Myc-Skp1 and HA-Rbx1. The SCF^{Skp2} E3 complexes were purified from the WCLs using anti-Flag-M2 agarose. Briefly, GST-IDH1-WT and GST-IDH1-T157A were expressed in BL21 *E.coli* and purified using Glutathione Sepharose 4B according to the manufacturer's instructions. Purified, recombinant GST-IDH1-WT and GST-IDH1-T157A proteins were incubated with purified SCF^{Skp2} complexes in the presence of purified, recombinant active E1, E2 (UBCH5A and UBCH3), cyclin E/CDK2, cyclin A/CDK2, ATP and ubiquitin. The reactions were stopped by the addition of 2× SDS-PAGE sample buffer, and the reaction products were resolved by SDS-PAGE and probed with the indicated antibodies.

Cycloheximide chasing assay
To determine the half-life of IDH1 protein, cells were treated with 200 μg/mL of cycloheximide and harvested at the indicated time points, and the cell lysate was then subjected to SDS-PAGE and IB of the indicated proteins.

FACS analysis
Cells that were synchronized with nocodazole and released were collected at the indicated time points and stained with propidium iodide (PI) according to the manufacturer's instructions. Stained cells were analyzed with a Dako-Cytomation MoFlo sorter (Dako).

Peptide-binding assay
The IDH1 peptides with/without phosphorylation modification were synthesized in LifeTein, LLC (Somerset, New Jersey, USA). Each peptide contained an N-terminal biotin and free C-terminus. The peptides were diluted into 1 mg/mL for further biochemical assays. The sequences were listed below:

IDH1 Biotin-TDFVVPGPGKVEITYTPSDGTQKVTYLVHNF.
pIDH1 Biotin-TDFVVPGPGKVEITYT(p)PSDGTQKVTYLVHNF.
IDH2 Biotin-TDFVADRAGTFKMVFTPKDGSGVKEWEVYNF.
pIDH2 Biotin-TDFVADRAGTFKMVFT(p)PKDGSGVKEWEVYNF.

Peptides (2 μg) were incubated with 10 μg of recombinant Skp2 proteins for 4 h at 4 °C, and 10 μL Streptavidin agarose was added in the sample for another 1 h. The agarose was washed four times with NETN buffer. Bound proteins were added in 2× SDS-PAGE loading buffer and resolved by SDS-PAGE for IB analysis.

Mass spectrometry analysis
Mass spectrometry analysis was performed as described previously with minor modifications.[26] Briefly, anti-Flag-IDH1 immunoprecipitations were performed with the WCLs derived from three 10-cm dishes of HEK293 cells co-transfected with Flag-IDH1, HA-cyclin E and HA-CDK2. The immunoprecipitated proteins were resolved by SDS-PAGE, and stained by Gelgold staining buffer. The band containing IDH1 was reduced with 10 mM DTT for 30 min, alkylated with 55 mM iodoacetamide for 45 min, and in-gel digested with trypsin. The resulting peptides were extracted from the gel and analyzed by microcapillary reversed phase liquid chromatography-tandem mass spectrometry (LC-MS/MS) using a high resolution Orbitrap Elite (Thermo Fisher Scientific) in positive ion DDA mode via CID, as previously described. MS/MS data were searched against the human protein database using Mascot (Matrix Science) and data analysis was performed using the Scaffold 4 software.

Clonogenic survival and soft agar assay
Cells were cultured in 10% FBS-containing DMEM or RPMI-1640 media before being plated into 6-well plate with 10,000 cells (3000 cells for HeLa) per well. Ten days later, cells were fixed with 10% acetic acid/10% methanol for 10 min, stained with 0.4% crystal violet/20% ethanol, followed by counting of the colony numbers. For soft agar assays, cells were seeded in 0.4% low-melting-point agarose in DMEM or RPMI-1640 containing 10% FBS with 100,000 per well (30,000 cells for HeLa), and layered onto 0.8% agarose in DMEM or RPMI-1640 with 10% FBS. The plates were kept in the cell culture incubator for 3–4 weeks after which the cells were stained with iodonitrotetrazolium chloride and colonies were counted.

Extraction of labeled metabolites
U-^{13}C6-glucose-labeled DMEM was prepared with non-glucose, non-glutamine and non-pyruvate DMEM by adding 10 mM of U-^{13}C6 D-glucose, 1 mM sodium pyruvate and 2 mM glutamine. U-^{13}C5-glutamine-labeled DMEM was prepared with non-glucose, non-glutamine and non-pyruvate DMEM by adding 2 mM of U-^{13}C5 glutamine, 1 mM sodium pyruvate and 25 mM glucose. ^{13}C flux assay was performed according to the previous report.[38] Briefly, medium was refreshed 1 h before cell harvest to remove accumulated metabolic wastes. For metabolite labeling, before harvesting sample, the cells were changed to U-^{13}C6-glucose-labeled media for labeling for 30, 60 and 120 s or U-^{13}C5-glutamine-labeled media for labeling for 1, 2 and 3 h. The medium was aspirated completely and 4 mL of dry ice cold 80% MeOH was added, followed by placing of the plates at −80 °C for 30 min. Then the metabolites were extracted as previously described and normalized by protein amount. All metabolites were analyzed as previously described.[20]

Glucose and glutamine uptake
The uptakes of glucose and glutamine for HeLa cells in either G1 phase or S phase were measured using Glucose Uptake Cell-Based Assay Kit and Glutamate Assay kit according to the manufacturer's protocol. For glucose uptake, cells were stained with 2-NBDG followed by flow cytometry analysis (excitation/emission = 485/538 nm). For glutamine uptake, cells were harvested and analyzed for OD_{450}.

Fractionation of cytoplasm, mitochondria and nuclei
Cells were harvested and subjected to fractionation of cytoplasm, mitochondria, and nuclei using Cell Fractionation kit. All fractions and the WCL were subjected to IB analysis of the indicated proteins, with tubulin, citrate synthase, and Histon H3 as markers of cytoplasm, mitochondria, and nuclei, respectively.

qPCR
Cells were harvested and the total RNA was extracted with TRIzol (Thermo Fisher Scienctific). The RNA was reverse-transcribed (PrimeScript RT Master Mix, RR036A, Takara) and target genes were analyzed with qPCR (FastStart Universal SYBR Green Master, 04913914001, Roche) using the CFX realtime PCR system (BioRad). *GAPDH* were used as internal control.

Xenograft assays in nude mice
22Rv1 cells stably expressing HA-IDH1-WT or HA-IDH1-T157A were inoculated into the flank of male nude mice (5×10^6 cells per injection, 7–8 mice for each group). After 4 weeks, the mice were sacrificed humanely, and the xenograft tumors were dissected and weighed.

Statistical analysis
The statistical significance between experimental groups was determined by Student's *t*-test or one-way ANOVA. The threshold for statistical significance was set to $P < 0.05$.

ACKNOWLEDGEMENTS
This work was supported in part by the NIH grants (CA229307 and CA200573 to W.W.; CA183914 to L.W.; R01CA068490, P50CA101942 and R35CA210068 to W.G.K.), the National Basic Research Program of China (2015CB553602 to J.K.L.; 2015CB856302 to J.G. L.), the National Natural Science Foundation of China (91649106, 31570777, 31770917 and 31700684 to J.K.L.; 81802787 to Y.P.). Fundamental Research Funds for the Central Universities (08143008 and 08143101 to J.K.L.; zrzd2017013 to J.G.L.) and American Cancer Society (to H.J.). We thank Wangxiao He, Zhanwu Hou and Huadong Liu for their help with the peptide synthesis, thank Evan Chen for his kind help with metabolite labeling, and thank Brian J. North and Wei lab members for critical reading of the manuscript, and members of the Wei, Pandolfi, Kaelin and Liu laboratories for helpful discussions.

AUTHOR CONTRIBUTIONS
J.L. and Y.P. designed and performed most of the experiments with assistance from L.S., L.W., H.J., J.G.L., J.P.G., J.Z., S.Z., X.W., J.G., X.D., S.F. and L.J., M.Y. and J.M.A. performed the LC-MS/MS metabolomic profiling and mass spectrometry analysis of IDH1 T157 phosphorylation. W.W., J.K.L., P.P.P., and W.G.K. supervised the study. J.L. and W.W. wrote the manuscript. All authors commented on the manuscript.

ADDITIONAL INFORMATION
Supplementary information accompanies this paper at https://doi.org/10.1038/s41422-020-0372-z.

Competing interests: W.W. is a co-founder and consultant of the ReKindle Therapeutics. All other authors declare no competing interests.

REFERENCES

1. Warburg, O. On the origin of cancer cells. *Science* **123**, 309–314 (1956).
2. Vander Heiden, M. G., Cantley, L. C. & Thompson, C. B. Understanding the Warburg effect: the metabolic requirements of cell proliferation. *Science* **324**, 1029–1033 (2009).
3. Bensaad, K. et al. TIGAR, a p53-inducible regulator of glycolysis and apoptosis. *Cell* **126**, 107–120 (2006).
4. Gordan, J. D., Thompson, C. B. & Simon, M. C. HIF and c-Myc: sibling rivals for control of cancer cell metabolism and proliferation. *Cancer Cell* **12**, 108–113 (2007).
5. Manning, B. D. & Cantley, L. C. AKT/PKB signaling: navigating downstream. *Cell* **129**, 1261–1274 (2007).
6. Christofk, H. R. et al. The M2 splice isoform of pyruvate kinase is important for cancer metabolism and tumour growth. *Nature* **452**, 230–233 (2008).
7. Wang, H. et al. The metabolic function of cyclin D3-CDK6 kinase in cancer cell survival. *Nature* **546**, 426–430 (2017).
8. Hanahan, D. & Weinberg, R. A. Hallmarks of cancer: the next generation. *Cell* **144**, 646–674 (2011).
9. Tu, B. P., Kudlicki, A., Rowicka, M. & McKnight, S. L. Logic of the yeast metabolic cycle: temporal compartmentalization of cellular processes. *Science* **310**, 1152–1158 (2005).
10. Chen, Z., Odstrcil, E. A., Tu, B. P. & McKnight, S. L. Restriction of DNA replication to the reductive phase of the metabolic cycle protects genome integrity. *Science* **316**, 1916–1919 (2007).
11. Tudzarova, S. et al. Two ubiquitin ligases, APC/C-Cdh1 and SKP1-CUL1-F (SCF)-beta-TrCP, sequentially regulate glycolysis during the cell cycle. *Proc. Natl. Acad. Sci. USA* **108**, 5278–5283 (2011).
12. Colombo, S. L. et al. Anaphase-promoting complex/cyclosome-Cdh1 coordinates glycolysis and glutaminolysis with transition to S phase in human T lymphocytes. *Proc. Natl. Acad. Sci. USA* **107**, 18868–18873 (2010).
13. Bao, Y. et al. Energy management by enhanced glycolysis in G1-phase in human colon cancer cells in vitro and in vivo. *Mol. Cancer Res.* **11**, 973–985 (2013).
14. Benanti, J. A., Cheung, S. K., Brady, M. C. & Toczyski, D. P. A proteomic screen reveals SCFGrr1 targets that regulate the glycolytic–gluconeogenic switch. *Nat. Cell Biol.* **9**, 1184–1191 (2007).
15. Herrero-Mendez, A. et al. The bioenergetic and antioxidant status of neurons is controlled by continuous degradation of a key glycolytic enzyme by APC/C–Cdh1. *Nat. Cell Biol.* **11**, 747–752 (2009).
16. Almeida, A., Bolaños, J. P. & Moncada, S. E3 ubiquitin ligase APC/C-Cdh1 accounts for the Warburg effect by linking glycolysis to cell proliferation. *Proc. Natl. Acad. Sci. USA* **107**, 738–741 (2010).
17. Sakamaki, T. et al. Cyclin D1 determines mitochondrial function in vivo. *Mol. Cell Biol.* **26**, 5449–5469 (2006).
18. Shimizu, K. et al. The SCFβ-TRCP E3 ubiquitin ligase complex targets Lipin1 for ubiquitination and degradation to promote hepatic lipogenesis. *Sci. Signal.* **10**, eaah4117 (2017).
19. Pavlova, N. N. & Thompson, C. B. The emerging hallmarks of cancer metabolism. *Cell Metab.* **23**, 27–47 (2016).
20. Yuan, M., Breitkopf, S. B., Yang, X. & Asara, J. M. A positive/negative ion-switching, targeted mass spectrometry-based metabolomics platform for bodily fluids, cells, and fresh and fixed tissue. *Nat. Protoc.* **7**, 872–881 (2012).
21. Srere, P. A. Complexes of sequential metabolic enzymes. *Annu. Rev. Biochem.* **56**, 89–124 (1987).
22. Kim, S. et al. Suppression of tumorigenesis in mitochondrial NADP+-dependent isocitrate dehydrogenase knock-out mice. *Biochim. Biophys. Acta* **1842**, 135–143 (2014).
23. Itsumi, M. et al. Idh1 protects murine hepatocytes from endotoxin-induced oxidative stress by regulating the intracellular NADP(+)/NADPH ratio. *Cell Death Differ.* **22**, 1837–1845 (2015).
24. Gohil, V. M. et al. Nutrient-sensitized screening for drugs that shift energy metabolism from mitochondrial respiration to glycolysis. *Nat. Biotechnol.* **28**, 249–255 (2010).
25. Wang, Z., Liu, P., Inuzuka, H. & Wei, W. Roles of F-box proteins in cancer. *Nat. Rev. Cancer* **14**, 233–247 (2014).
26. Liu, P. et al. Cell-cycle-regulated activation of Akt kinase by phosphorylation at its carboxyl terminus. *Nature* **508**, 541–545 (2014).
27. Koff, A. et al. Formation and activation of a cyclin E-cdk2 complex during the G1 phase of the human cell cycle. *Science* **257**, 1689–1694 (1992).
28. Zhang, H., Kobayashi, R., Galaktionov, K. & Beach, D. p19skp1 and p45skp2 are essential elements of the cyclin A-CDK2 S phase kinase. *Cell* **82**, 915–925 (1995).
29. Lin, H. K. et al. Skp2 targeting suppresses tumorigenesis by Arf-p53-independent cellular senescence. *Nature* **464**, 374–379 (2010).
30. Wu, L. et al. Specific small molecule inhibitors of Skp2-mediated p27 degradation. *Chem. Biol.* **19**, 1515–1524 (2012).
31. Carrano, A. C., Eytan, E., Hershko, A. & Pagano, M. SKP2 is required for ubiquitin-mediated degradation of the CDK inhibitor p27. *Nat. Cell Biol.* **1**, 193–199 (1999).
32. Donato, V. et al. The TDH–GCN5L1–Fbxo15–KBP axis limits mitochondrial biogenesis in mouse embryonic stem cells. *Nat. Cell Biol.* **19**, 341–351 (2017).
33. Owusu-Ansah, E., Yavari, A., Mandal, S. & Banerjee, U. Distinct mitochondrial retrograde signals control the G1-S cell cycle checkpoint. *Nat. Genet.* **40**, 356–361 (2008).
34. Inuzuka, H. et al. Acetylation-dependent regulation of Skp2 function. *Cell* **150**, 179–193 (2012).
35. Carette, J. E. et al. Haploid genetic screens in human cells identify host factors used by pathogens. *Science* **326**, 1231–1235 (2009).
36. Sanjana, N. E., Shalem, O. & Zhang, F. Improved vectors and genome-wide libraries for CRISPR screening. *Nat. Methods* **11**, 783–784 (2014).
37. Boehm, J. S., Hession, M. T., Bulmer, S. E. & Hahn, W. C. Transformation of human and murine fibroblasts without viral oncoproteins. *Mol. Cell Biol.* **25**, 6464–6474 (2005).
38. Wan, L. et al. APCCdc20 suppresses apoptosis through targeting Bim for ubiquitination and destruction. *Dev. Cell* **29**, 377–391 (2014).
39. Wei, W. et al. Degradation of the SCF component Skp2 in cell-cycle phase G1 by the anaphase-promoting complex. *Nature* **428**, 194–198 (2004).
40. Inuzuka, H. et al. SCF FBW7 regulates cellular apoptosis by targeting MCL1 for ubiquitylation and destruction. *Nature* **471**, 104–109 (2011).